Supplementary Information for

Topochemical Synthesis of Perovskite-type CuNb$_2$O$_6$ with Colossal Dielectric Constant

Masayuki Fukuda,[*ab] Ikuya Yamada,[c] Hajime Hojo,[d] Chihiro Takahashi,[a] Yuya Yoshida,[a] Katsuhisa Tanaka,[a] Masaki Azuma[b] and Koji Fujita[*a]

a Department of Material Chemistry, Graduate School of Engineering, Kyoto University, Kyoto 615-8510, Japan
b Laboratory for Materials and Structures, Tokyo Institute of Technology, Kanagawa 226- 8503, Japan
c Department of Materials Science, Graduate School of Engineering, Osaka Prefecture University, Osaka 599-8531, Japan
d Department of Advanced Materials Science and Engineering, Faculty of Engineering Sciences, Kyushu University, Fukuoka 816-8580, Japan

Sample preparation for the dielectric measurements

To evaluate the dielectric property of Pv-CuNb$_2$O$_6$, we first attempted to obtain rigid pellets by compressing with a conventional press at ~10 MPa and subsequent sintering in ambient conditions. However, Pv-CuNb$_2$O$_6$ was found to transform into a monoclinic columbite-type structure at about 950 K (Fig. S1). Therefore, sintering was carried out at lower temperature (773 K) for 24–48 h, but the resultant pellet was too fragile with a relative density of less than 70 % to perform the dielectric experiments. Next, we tried to prepare the dense pellets by compressing the powdered specimen of Pv-CuNb$_2$O$_6$ at 3 GPa using our high-pressure apparatus. The compressed pellets were sintered in air for 24 h at 773 K and ambient pressure, getting sufficiently dense with a relative density of ~86 %. It has been reported that some A-site deficient perovskites exhibit irreversible pressure-induced amorphization at room temperature (e.g. R$_{1/3}$NbO$_3$ at 14.5 GPa and R$_{1/3}$TaO$_3$ at 18.5 GPa (R = La, Pr, Nd)).[1–3] Then, we confirmed using XRD data that no amorphization occurred at 3 GPa for Pv-CuNb$_2$O$_6$.
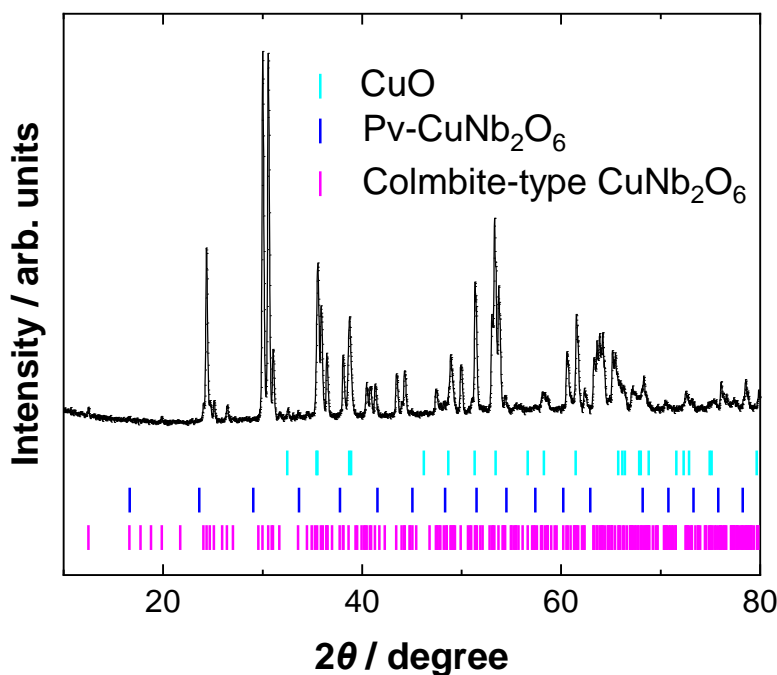

Fig. S1. Laboratory XRD pattern (CuKα) measured at room temperature after annealing of high-pressure-synthesized Pv-CuNbO$_3$ at 973 K. The light blue, blue and magenta ticks correspond to the Bragg positions for CuO and Pv-CuNb$_2$O$_6$ and monoclinic columbite-type CuNb$_2$O$_6$, respectively.

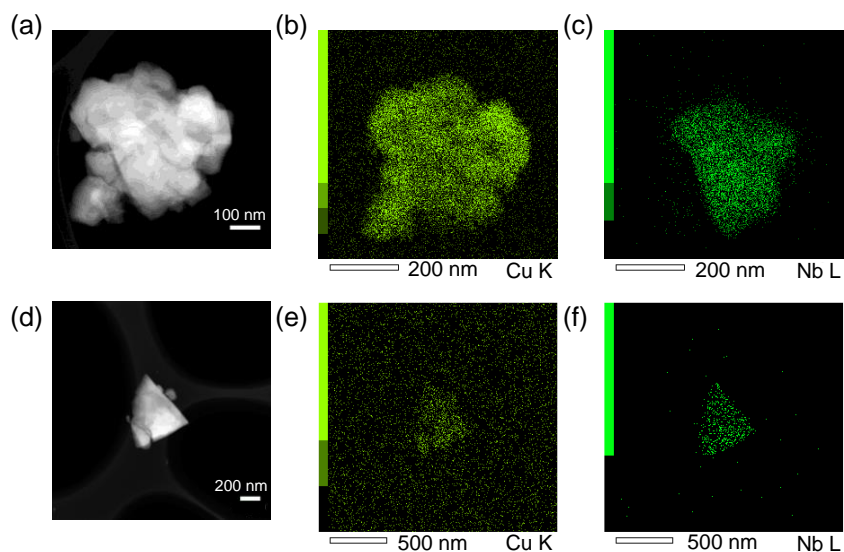**The topochemical reaction after the post-annealing or the heating cycle of TG-DTA experiment**

Fig. S2. HAADF-STEM images for the post-annealed mixture grains of Pv-CuNb$_2$O$_6$ and CuO. (a) and (d) represent the appearance of grain 1 and grain 2, respectively. (b) Cu and (c) Nb EDX mapping for the grain 1, and (e) Cu and (f) Nb EDX mapping for the grain 2. The association of the smaller grains containing only Cu atom (CuO) on the larger grains containing both Cu and Nb atoms (Pv-CuNb$_2$O$_6$) is observed.
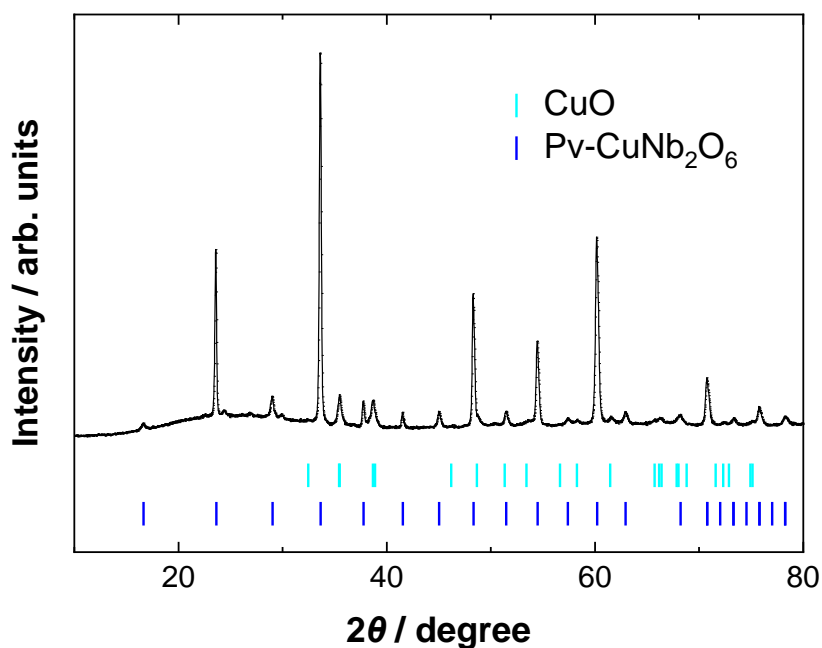

Fig. S3. Laboratory XRD pattern (CuKα) measured at room temperature after heating of high-pressure-synthesized Pv-CuNbO$_3$ to 673 K in the TG-DTA experiment. The light blue and blue ticks correspond to the Bragg positions for CuO and Pv-CuNb$_2$O$_6$, respectively.
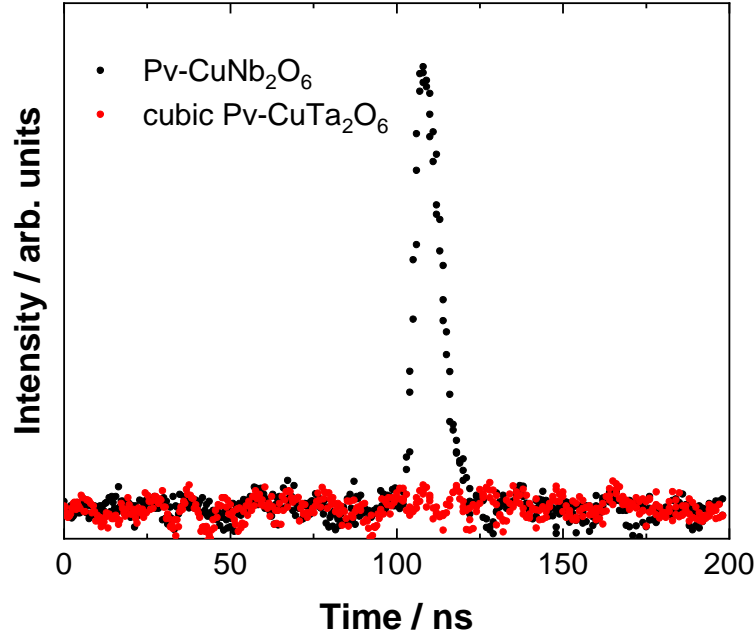
Characterizations of Pv-CuNb₂O₆

- • Pv-CuNb$_2$O$_6$
- • cubic Pv-CuTa$_2$O$_6$

Fig. S4. Oscilloscope traces of the SHG signals for Pv-CuNb$_2$O$_6$ and quenched cubic Pv-CuTa$_2$O$_6$ (centrosymmetric reference) at room temperature.
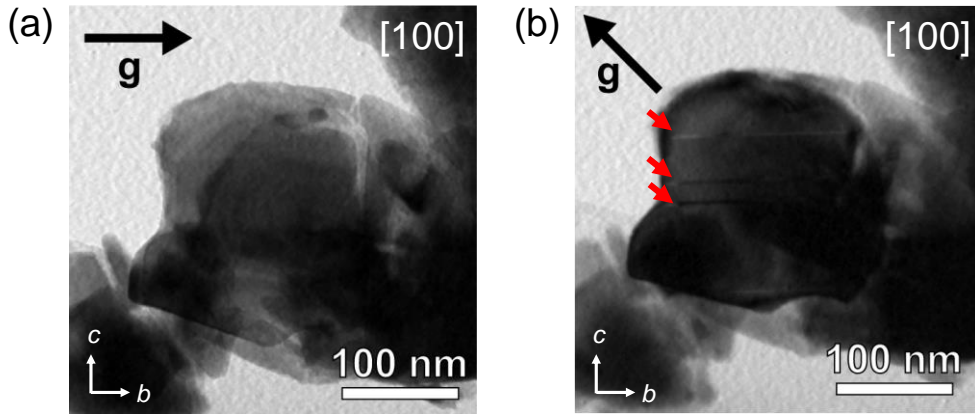

Fig. S5. TEM BF images of [100]-oriented Pv-CuNb$_2$O$_6$. The diffraction vector, g, is set to in-plane (a) [010] and (b) [0$\bar{1}$1]. The red arrows in (b) represent the domain structures. Only when we observed with $g = 0\bar{1}1$, domain structures perpendicular to the c-axis (red arrows in (b)) can be observed.

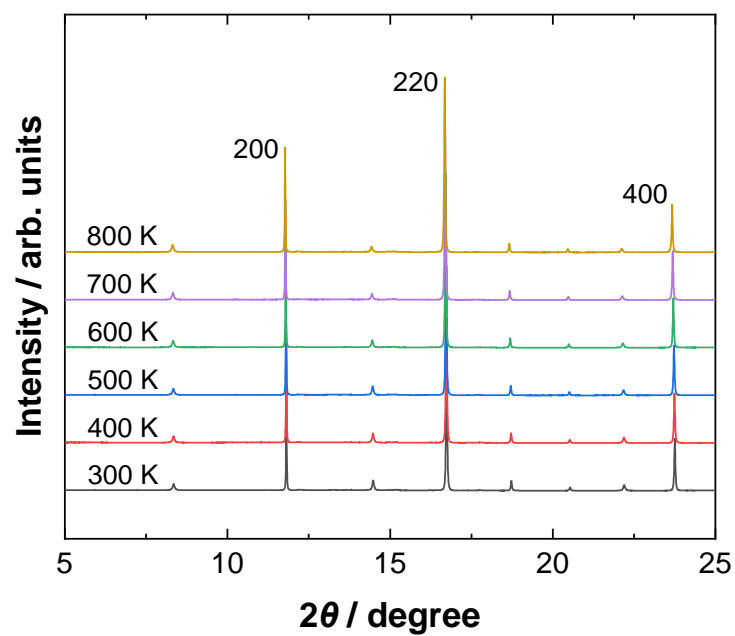Fig. S6. Temperature evolution of SXRD patterns (λ = 0.77443 Å) of Pv-CuNb$_2$O$_6$ in the temperature range of 300 to 800 K.

Table S1. Refined composition, crystal symmetry, lattice volume, bond lengths, bond angles and BVS for $CuNb_2O_6$, and those for $CuTa_2O_6$ and $LiCuNb_3O_9$ as previously reported[4,5].

	$CuNb_2O_6$		$CuTa_2O_6$		$LiCuNb_3O_9$	
Refined composition	$Cu_{1.02}Nb_2O_6$		$Cu_{1.01}Ta_2O_6$		$LiCuNb_3O_9$	
Crystal symmetry	cubic $I23$		cubic $Pm\bar{3}$		cubic $I23$	
V /Å^3	426.13		419.69		426.72	
Bond length /Å	Cu1—O1	2.021(4) × 4	Cu1—O2	2.033(3) × 4	Cu1—O1	2.02(2) × 4
			Cu2—O1	2.033(3) × 4		
	Nb1—O1	1.903(5) × 3	Ta1—O1	1.974(2) × 3	Nb1—O1	1.92(3) × 3
	—O1	2.079(5) × 3	—O2	1.977(2) × 3	—O1	2.07(3) × 3
Bond Angles / °	Nb1—O1—Nb1	142.2(2)	Ta1—O1—Ta1	143.0(2)	Nb1—O1—Nb1	142.2(10)
			Ta1—O2—Ta1	142.4(2)		
BVS	Cu1	1.9	Cu1	1.9	Cu1	1.6
			Cu2	1.9		
	Nb1	5.0	Ta1	5.2	Nb1	4.9
References	This work		4		5	

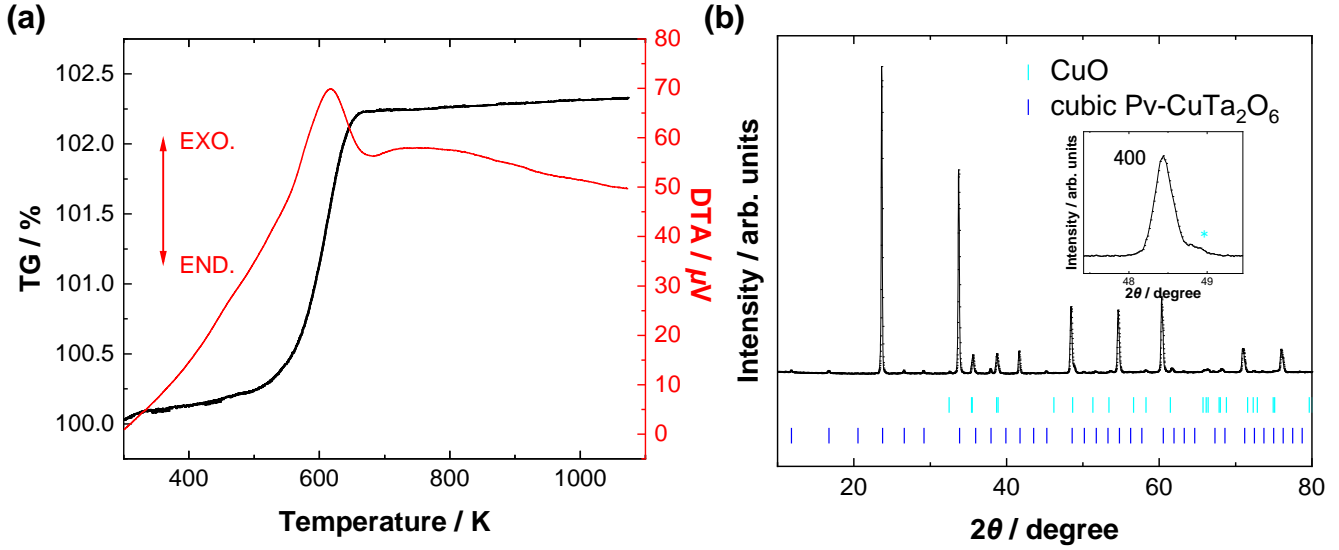# Characterizations of Pv-CuTa₂O₆

(a)

(b)

Fig S7. (a) TG-DTA curves measured between 300 and 1073 K for high-pressure-synthesized Pv-CuTaO$_3$. The exothermic peak with ~2 % weight gain (estimated by subtracting background level) was observed at around 600 K, corresponding to the topochemical reaction: CuTaO$_3$ + 0.19O$_2$ → 0.38CuO + Cu$_{1.24}$Ta$_2$O$_6$. (b) Laboratory XRD pattern (CuKα) measured at room temperature after heating of high-pressure-synthesized Pv-CuTaO$_3$ to 1073 K in the TG-DTA experiment. The light blue and blue ticks correspond to the Bragg positions for CuO and Pv-CuTa$_2$O$_6$, respectively. The inset is an enlarged view of 400 peak from Pv-CuTa$_2$O$_6$, indicating that there is no peak splitting. The light blue asterisk in the inset corresponds to a peak from CuO.
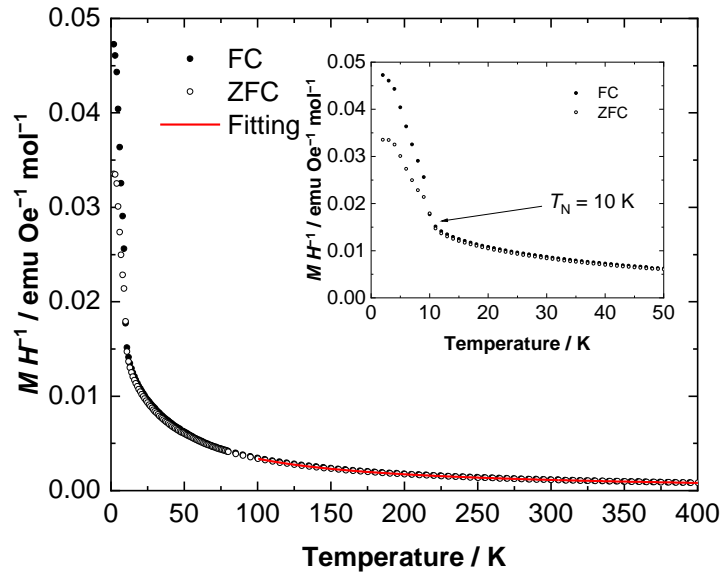

Fig. S8. Temperature dependence of magnetic susceptibility, $\chi = M\,H^{-1}$, of the quenched cubic Pv-CuTa$_2$O$_6$ measured at H = 100 Oe after field cooling (FC) and zero-field cooling (ZFC). The inset features a magnified view near the antiferromagnetic transition temperature. The black filled and open circles represent the observed FC and ZFC data, whereas the red solid line is the fitted curve based on the Curie-Weiss law, $\chi = \chi_0 + C / (T - \theta_W)$. We obtained χ_0 = $-1.49(6) \times 10^{-4}$ emu Oe^{-1} mol^{-1}, C = 0.402(3) emu K Oe^{-1} mol^{-1} and $\theta_W = -13.8(6)$ K.
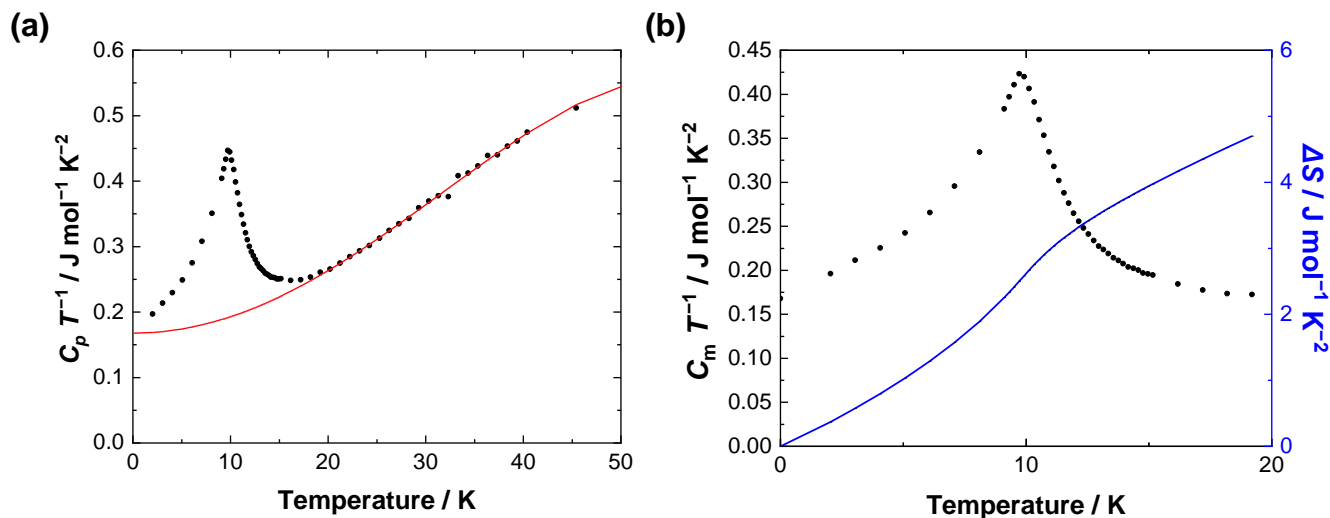
Fig. S9. (a) The specific heat divided by temperature, $C_p T^{-1}$ (black dots) and the fitting results of the lattice specific heat for quenched cubic Pv-CuTa$_2$O$_6$ (solid red line), based on the following equation below 50 K, $C/T = \gamma + \beta_1 T^2 + \beta_2 T^4$. (b) The magnetic specific heat divided by temperature, $C_m T^{-1}$ (black dots), and the magnetic entropy (solid blue line) below 20 K. We obtained the calculated values, $\gamma = 0.168(4)$ J mol^{-1} K^{-2}, $\beta_1 = 2.55(7) \times 10^{-4}$ J mol^{-1} K^{-4} and $\beta_2 = -4.2(2) \times 10^{-8}$ J mol^{-1} K^{-6} and $\Delta S = 4.7$ J mol^{-1} K^{-1}.

References

[1] O. Noked, S. Yakovlev, Y. Greenberg, G. Garbarino, R. Shuker, M. Avdeev and E. Sterer, *J. Non-Cryst. Solids* 2011, **357**, 3334–3337.

[2] O. Noked, A. Melchior, R. Shuker, T. Livneh, R. Steininger, B. J. Kennedy and E. Sterer, *J. Solid State Chem*. 2013, **202**, 38–42.

[3] O. Noked, A. Melchior, R. Shuker, R. Steininger, B. J. Kennedy and E. Sterer, *Phys. Chem. Miner.*, 2014, **41**, 439–447.

[4] V. Propach, *Z. Anorg. Allg. Chem.,* 1977, **435**, 161–171.

[5] M. Sato and Y. Hama, *J. Mater. Chem.*, 1993, **3**, 233–236.